Available online at www.sciencedirect.com
ScienceDirect
Journal of Molecular Graphics and Modelling 25 (2006) 562–577
Journal of Molecular Graphics and Modelling
www.elsevier.com/locate/JMGM

Docking studies of agonists and antagonists suggest an activation pathway of the A_3 adenosine receptor

Soo-Kyung Kim [a], Zhan-Guo Gao [a], Lak Shin Jeong [b], Kenneth A. Jacobson [a,*]

[a] *Molecular Recognition Section, Laboratory of Bioorganic Chemistry, National Institute of Diabetes and Digestive and Kidney Diseases (NIDDK), National Institutes of Health (NIH), Bethesda, MD 20892, USA*

[b] *Laboratory of Medicinal Chemistry, College of Pharmacy, Ewha Womans University, Seoul 120-750, South Korea*

Received 22 March 2006; received in revised form 3 May 2006; accepted 3 May 2006
Available online 9 May 2006

Abstract

Structural determinants of ligand efficacy in the human A_3 adenosine receptor (AR) were studied using pharmacophore and docking analyses of various categories of A_3 selective ligands: inverse agonist, neutral antagonist (nonnucleoside and nucleoside), and agonist (partial and full). The homology modeling of GPCRs was adapted to provide two templates: the rhodopsin-based resting state for antagonist binding and a putative Meta I state, conformationally altered at a key residue (W6.48), for agonist binding. The preferential binding domains and/or local conformational changes associated with docking of three high affinity A_3AR ligands were compared: inverse agonist PSB-11 **1** ((*R*)-8-ethyl-4-methyl-2-phenyl-imidazo[2,1-i]purin-5-one); neutral antagonist MRE-3008F20 **7** (5-[[(4-methoxyphenyl)amino]carbonyl]amino-8-methyl-2-(2-furyl)pyrazolo[4,3-e]1,2,4-triazolo[1,5-c]pyrimidine), and full agonist Cl-IB-MECA **21** (2-chloro-N^6-(3-iodobenzyl)-5′-*N*-methylcarboxamidoadenosine) to define a distinct recognition mode for each. Ribose-containing agonists were more hydrophilic than nonnucleoside antagonists, and H-bonding ability at the ribose 3′- and 5′-positions was required for agonism. From the receptor perspective, common requirements for activation included the destabilization of H-bond networks at W6.48 and H7.43, the specific interactions of the ribose moiety in its putative hydrophilic pocket at T3.36, S7.42, and H7.43, the stabilization of the complex by inward movement of F5.43, and the characteristic rotation of W6.48. By analogy, outward rotation of the W6.48 side-chain upon activation of an internally-crosslinking mutant M_3 muscarinic receptor was indicated by constrained molecular dynamics (MD). Our results are consistent with an anti-clockwise rotation (from the extracellular view) of transmembrane domains 3, 5, 6, and 7, as proposed for other Family A GPCRs. Thus, the putative conformational changes associated with A_3AR activation indicate a shared mechanism of GPCR activation similar to rhodopsin.

Keywords: Purines; G-protein-coupled receptor; Homology modeling; 7TM receptor; Binding site; Nucleoside

1. Introduction

Four subtypes of adenosine receptors (ARs), a rhodopsin-like Family A G-protein-coupled receptor (GPCR), have been important therapeutic targets for drug development [1]. Agonists of the A_3AR subtype act to prevent ischemic damage in the brain and heart, and have anti-inflammatory, anti-cancer and myeloprotective effects. The compound IB-MECA (N^6-(3-iodobenzyl)-5′-*N*-methylcarboxamidoadenosine), which we developed as a selective A_3AR agonist, has been in Phase II clinical studies for the treatment of metastatic colorectal tumors and rheumatoid arthritis [2,3].

However, there are major barriers to the clinical development of AR agonists. The ubiquitous expression of ARs in the body leads to diverse side effects, and the low receptor density in the targeted tissue limits the effect of drugs in certain diseases. A_3AR selective agonists have been described as promising cardio- and cerebroprotective agents. However, the low density of the A_3AR in the heart may be a problem [4]. In 2000, it was reported that one of the major causes of attrition in drug discovery, accounting for 28% of cases, was the lack of systemic drug efficacy [5]. Thus, to develop selective A_3AR agonists with the aid of molecular modeling, the structural requirements for subtype selectivity and the molecular properties required for

* Corresponding author at: Molecular Recognition Section, Bldg. 8A, Rm. B1A-19, NIH, NIDDK, LBC, Bethesda, MD 20892-0810, USA.
Tel.: +1 301 496 9024; fax: +1 301 480 8422.
E-mail address: kajacobs@helix.nih.gov (K.A. Jacobson).

1093-3263/$ – see front matter
doi:10.1016/j.jmgm.2006.05.004

agonism should be studied. Understanding the molecular mechanism involved in agonist binding and the accompanying conformational change of the A_3ARs is also crucial.

The 3D-structures of GPCRs provide important information for understanding their molecular organization and how agonists participate in conformational changes upon activation. However, obtaining the structural information about GPCRs through the application of standard structural determination techniques, X-ray, and NMR studies, has progressed slowly. The main reason has been the technical difficulty of large-scale receptor purification and the insolubility in media lacking phospholipids. However, since the X-ray structure of bovine rhodopsin (PDB ID: 1F88) was first published in 2000 [6], this structure has been widely applied to homology modeling, based on the hypothesis of structural mimicry, i.e. different amino acids or alternate microdomains can support similar deviations from a regular α-helical structure, thereby resulting in a similar tertiary structure [7].

To study the activation mechanism of GPCRs, several limitations of computer modeling as well as experimental approaches have been considered: (1) Currently, the unique template for generating 3D-models of GPCRs is the inactive form of bovine rhodopsin to which *cis*-retinal is covalently bound as an inverse agonist. The reliability of docking models of agonists is limited by using a ground-state template. (2) Although several computational models of the active state [8,9] have been proposed, these theoretical models all exhibited different conformations depending on the experimental data. Some models were not consistent with recent experimental results, e.g. the computational model did not show the predicted separation of the cytosolic extensions of TMs 3 and 6 [10]. (3) Explicit membrane/water added to a model makes it more difficult to perform molecular dynamics (MD) calculations with millisecond time scales in order to simulate the active states. (4) It is difficult to study drug efficacy with only a single snapshot from the several theoretically generated active conformations [8–10]. Receptors likely exist as collected ensembles of numerous conformations. Fluorescence spectroscopy studies of the β_2-adrenergic receptor provided evidence for a multi-step process of agonist binding, identifying the order of contacts between the receptor and key moieties [11]. A single agonist stabilizes a succession of conformational states with distinct cellular functions through induction or stabilization of multiple, functionally distinct conformational states. (5) The experimentally-determined relative efficacy of a given agonist may reflect interactions within higher order GPCR networks, a communication system through various interactions with the surroundings. The calculation may require considering the complexes of GPCR oligomers and G-proteins. Thus, a single active receptor model would not likely lead to an understanding of the efficacy of various ligands and the activation mechanism of a given GPCR.

However, the structure-activity relationship (SAR) of a wide range of adenosine derivatives at the A_3AR suggests the possibility of rationally "tuning" a desired selectivity and activity through structural modification [12,13]. Activation of the A_3AR depends on structural determinants of relative efficacy, independent of binding affinity, in adenosine derivatives. In this study, as depicted in Fig. 1, we compared

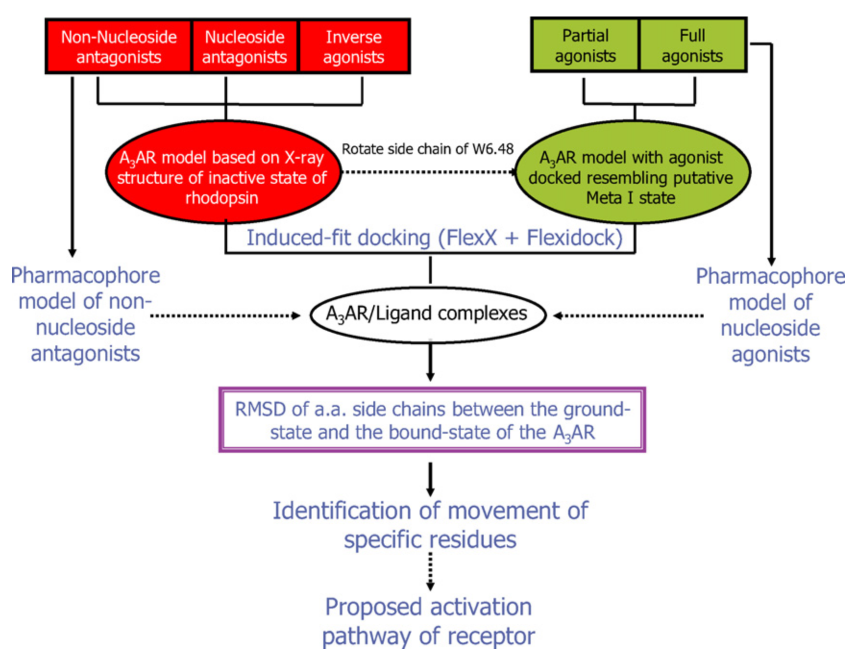

Fig. 1. A diagram showing the integration of pharmacophore analysis, receptor modeling, and ligand docking, as applied to various classes of A_3AR ligands. The homology model of the hA_3AR (PDB id: 1OEA) [12] was constructed using the X-ray structure of bovine rhodopsin with a 2.8 Å resolution (PDB id: 1F88) [6]. For the refinement of the side-chains, 500 ps molecular dynamics was performed with the constraints of the protein backbone atoms in the secondary structures. The average structure from the last 100-ps trajectory of MD was re-minimized with backbone constraints in the secondary structure and then without all constraints. The A_3AR conformations based on the X-ray structure of the resting state of rhodopsin and the putative Meta I state were used for antagonist docking and for agonist docking, respectively. For induced-fit docking study, automatic flexible docking methods facilitated through the FlexX and FlexiDock utilities in the Biopolymer module of SYBYL v7.0 were used. Finally, several complex structures were minimized and compared by using an Amber 7 force field 99.

antagonists and agonists according to their molecular properties and by phamacophore analysis. Complementary to ligand SAR, extensive mutagenesis studies, interpreted through AR homology modeling, have identified amino acids involved in ligand binding and activation [14]. In this study we have used the structural, pharmacological, and physical/chemical properties of these ligands to discern likely steps in the activation process.

We explored the different binding domain preferences and compared the specific interactions of representative A_3 selective ligands having three distinct functions, e.g. an inverse agonist, a neutral antagonist, and a full agonist. The difference in the preference of binding domain and/or local conformational change depended on the type of ligand docked. Representative antagonists were docked to an A_3AR conformation based on the X-ray structure of the resting state of rhodopsin, and agonists were docked to a putative Meta I state conformation of the A_3AR (Fig. 1). Thus, the A_3AR docking study of different categories of ligands provided a hypothetical mechanism of the initial conformational step(s) in receptor activation.

The agonist-bound conformation, in a form resembling the not fully-activated Meta I state of rhodopsin, was obtained by modeling the rearrangement of the side-chain of a key conserved Trp residue of ARs in transmembrane (TM) helical domain 6 (6.48). This rearrangement was required in order to dock various A_3AR agonists and was not required for antagonist docking. Although the Meta I state is still far more similar to the resting conformation than to the presumed, yet undisclosed fully active conformation, the Meta I state structure is preferable to the ground-state structure for agonist docking. The agonist-bound state of the A_3AR is similar to the Meta I state of rhodopsin, which is not the result of large rigid-body movements of helices, but rather a rearrangement of side-chains, especially 6.48, through a local conformational change in the binding site [15]. Consequent to the rearrangement of side-chains upon activation of GPCRs is the disruption of intramolecular interactions that constrain the receptor in the inactive state. Agonist binding to the A_3AR appears to disrupt the intramolecular H-bonding networks involving W6.48 and H7.43 and the specific interactions at highly conserved T3.36, S7.42, and H7.43, to induce a characteristic anti-clockwise movement of TMs 3, 6, and 7 from the extracellular view. Thus, we present novel insights into a putative activation mechanism of the A_3AR based on correlation of ligand recognition patterns in receptor docking and pharmacological function.

2. Results

2.1. Summary of relevant reported SAR of A_3AR antagonists and agonists

A number of adenosine derivatives have been developed as A_3AR selective agonists. Binding to the human A_3AR (hA_3AR) was characterized pharmacologically using a high affinity radioligand, [^{125}I]I-AB-MECA, and receptor activation was measured as the inhibition of forskolin-stimulated adenylate cyclase in intact CHO (Chinese hamster ovary) cells stably expressing this receptor [16].

2.1.1. Adenine substitutions

Although high binding affinity for the hA_3AR was obtained by the introduction of a 3-iodobenzyl substituent at the N^6-position, compound **14** displayed a relative efficacy of 46%, i.e. it was a partial A_3AR agonist. Combining a N^6-3-iodobenzyl moiety with a chlorine at the 2-position of compound **8** did not affect or slightly increased the binding affinity at the hA_3AR but dramatically decreased its agonist activity leading to 0% efficacy. The combination of N^6-benzyl and various 2-substitutions (chloro, iodo, methylcarboxylate, trifluoromethyl, and cyano) generally resulted in null efficacy at the A_3AR, whereas the N^6-methyl adenosine derivatives with 2-cyano or 2-trifluromethyl groups were full agonists [17]. Compound **9**, N^6-(2,2-diphenylethyl)adenosine, was an A_3AR antagonist, whereas the closely related compound **25** with a phenyl ring-constrained fluorenylmethyl group at the N^6-position was a full agonist. A conformationally constrained analogue, N^6-(1*S*,2*R*)-(2-phenyl-1-cyclopropyl)adenosine **24**, was highly increased in binding affinity to the hA_3AR with a K_i value of 0.63 nM [18].

2.1.2. Ribose ring modification

The N^6-(3-iodobenzyl) analogue **20** and its corresponding 2-chloro derivative Cl-IB-MECA **21**, both having 5′-*N*-methyluronamide groups, displayed enhanced binding affinity with K_i values of 1.8 and 1.4 nM, respectively. Ring-constrained methanocarba adenosine analogues, e.g. **22** and **23**, retain high affinity and selectivity for the A_3AR, with a North (N)/South (S) affinity ratio of 150, through stabilizing an active receptor-bound conformation, i.e. a (N) and anti-conformer [19]. Introduction of rigidity in the ribose of compound **20** increased the A_3AR selectivity by 10-fold (i.e. increase in A_1/A_3 ratio for compound **22**).

However, in the 5′-CH_2OH series, ring-constrained (*N*)-methanocarba adenine nucleosides with a N^6-benzyl group, e.g. **14**, tended to display reduced A_3AR efficacy. Alkylthio substituents at the 5′-position also induced partial agonism at the A_3AR [20]. However, a 5′-uronamide group restored efficacy, in spite of the presence of an efficacy-reducing structural feature elsewhere on the molecule. Additional experiments suggest that the flexibility and presence of H-bonding groups of the 5′-substituent are a major factor for full activation of the A_3AR. A cyclized spiral 4′,5′-uronamide derivative **10** was reported as an antagonist [12]. Similarly, for nucleoside antagonist **11**, appending a second *N*-methyl group on the 5′-uronamide position precluded activation of the A_3AR [21].

Both 2′- and 3′-hydroxyl groups in the ribose moiety contribute to A_3AR binding and activation. The 2′,3′-epoxy derivative of adenosine lost binding to the A_3AR. 2′-Fluoro substitution totally eliminated both binding and activation, while 3′-fluoro substitution led to only a partial reduction of binding affinity, but no agonist function at the A_3AR. The 5′-uronamide group, known to restore full efficacy in other derivatives, failed to fully overcome the diminished efficacy of 3′-fluoro derivatives such as **12**. Interestingly, a shift of the

Table 1
The binding affinities and relative efficacy (inhibition of adenylate cyclase as a percent of full agonist **20**) of various ligands at the human A_3AR expressed in CHO (Chinese hamster ovary) cells

#	Binding affinity K_i (hA_3AR), nM	Efficacy (% at 10 μM)	Predicted $C \log P$	Reference
1	2.3	–	2.75	[28]
2	0.79	0	1.85	[24]
3	18.9	0	6.91	[50]
4	0.6	0	0.4	[25]
5	2.7	0	6.61	[51]
6	0.65	0	4.54	[51]
7	0.2	0	3.70	[29]
8	1.8	0	1.97	[12]
9	3.9	0	2.21	[23]
10	29.3	0	0.28	[12]
11	29.0	0	1.69	[21]
12	406	0	1.77	[52]
13	4.3	0	1.74	[22]
14	5.8	46	1.24	[17]
15	290	100	−2.16	[53]
16	87	100	−1.44	[18]
17	26	100	−2.39	[3]
18	9.3	96	−1.33	[17]
19	3.4	101	−1.66	[17]
20	1.2	100	0.48	[4]
21	1.4	99	1.2	[18]
22	2.4	100	1.71	[23]
23	2.1	103	2.43	[12]
24	0.63	117	0.81	[18]
25	0.91	99	2.19	[18]

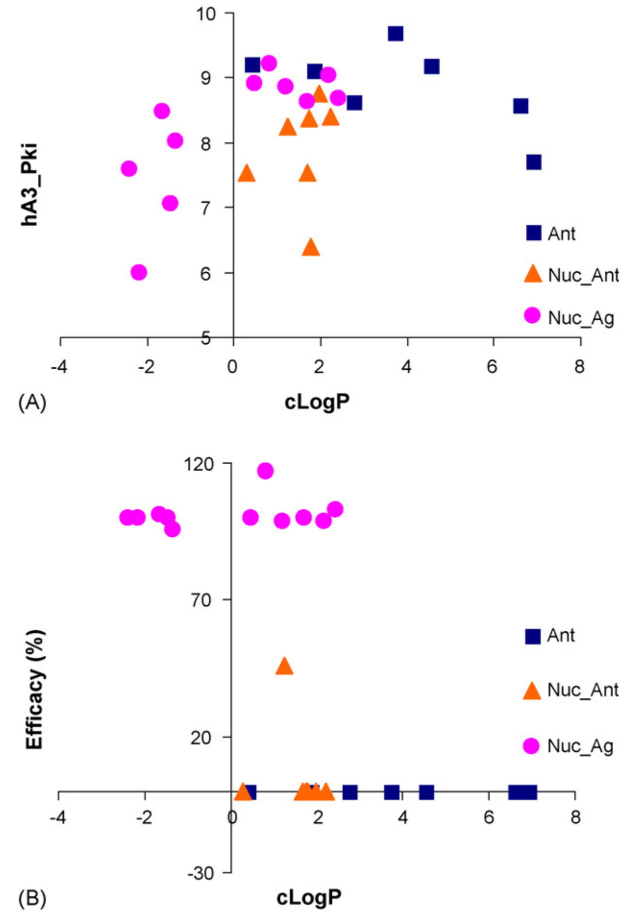

Fig. 2. Relation to pharmacological parameters of calculated $C \log P$ values for various nucleoside A_3AR agonists (●), nucleoside antagonists (▲), and nonnucleoside antagonists (■). (A) $C \log P$ vs. binding affinity (hA3_pKi = $-\log(hA_3K_i)$), (B) $C \log P$ vs. relative efficacy (%).

N^6-(3-iodobenzyl)adenine moiety from the 1′- to 4′-position in compound **13** had a minor influence on A_3AR selectivity, but no activation was observed [22].

The SAR studies concluded that structural features for reducing efficacy included N^6-benzyl and/or 2,2-diphenylethyl groups, small groups at C2 combined with N^6-bulky substituents, and sterically constrained moieties in the ribose region. For each of those efficacy-diminishing factors, a 5′-uronamide group tended to restore the observed loss of A_3AR efficacy [23].

2.2. Differences between molecular properties of nucleoside ligands and nonnucleoside antagonists

We compared physical properties of various A_3AR antagonists and agonists in Table 1. The calculated logarithm of the partition coefficient ($C \log P$), the equilibrium concentration of solute in a non-polar solvent divided by the concentration of the same solute species in a polar solvent, has been used as a measure of hydrophobicity. Most of the current potent and selective nonnucleoside A_3AR antagonists, including pyridines (**3** MRS1523), dihydropyridines (**5** MRS1334), triazoloquinazolines (**6** MRS1220), and pyrazolotriazolopyrimidines (**7** MRE-3008F20), have a high $C \log P$ (>3.7) and thus are highly lipophilic and display a very low degree of water-solubility. More water-soluble A_3AR antagonists, **2** [24] and **4** [25], are considered to be more tractable pharmacological tools for *in vitro* and *in vivo* studies. As displayed in Fig. 2, for A_3AR selective agonists, higher $C \log P$ values roughly correlated with higher binding affinity. The optimum $C \log P$ range for both agonist binding affinity and full efficacy was 0–2. Nucleoside antagonists of the A_3AR displayed a similar range of $C \log P$ values (0–2).

In summary, nonnucleoside antagonists displayed only a preference for $C \log P > 0$. Effective agonists tended to be more hydrophilic than nonnucleoside antagonists, due to the presence of the required ribose moiety, but the $C \log P$ values fell within narrowly defined limits. Nucleoside antagonists and agonists were similar in this respect.

2.3. Pharmacophore differences between agonists and nonnucleoside antagonists

A pharmacophore study contrasting hA_3AR selective agonists and nonnucleoside antagonists was performed using DISCO (DIStance COrrelation) analysis in SYBYL v. 7.0. Common pharmacophore features of the A_3AR selective antagonists in Chart 1 were detected within 1.25 Å tolerances, resulting in two aromatic centroids and two H-bond acceptor sites (Fig. 3A). The pharmacophore model of the A_3AR selective full agonists in Charts 2 and 3B included an H-bond

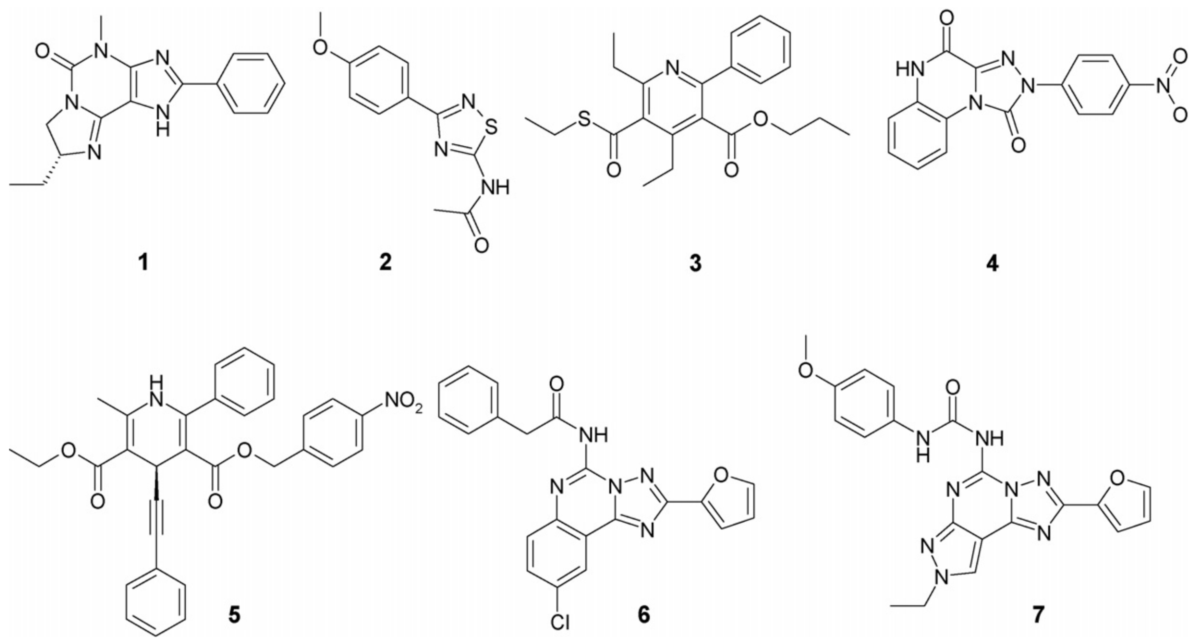

Chart 1. The structures of various nonnucleoside A_3AR antagonists. (**1**) tetrahydroimidazopurinone derivative PSB-11 (inverse agonist), (**2**) *N*-[3-(4-methoxy-phenyl)-[1,2,4]thiadiazol-5-yl]-acetamide, (**3**) pyridine derivative MRS1523, (**4**) triazoloquinoxalinedione derivative FA385, (**5**) 1,4-dihydropyridine derivative (4S)-MRS1334, (**6**) triazoloquinazoline derivative MRS1220, (**7**) pyrazolotriazolopyrimidine derivative MRE-3008F20.

donor at the 5′-position, an H-bond donor or acceptor at the 3′-O and the N^6 atoms, H-bond acceptors at the 2′ position, and at the N^1, N^3, and N^7 atoms of the adenine ring within 1 Å tolerance (Fig. 3B). Compared to the pharmacophore of the A_3AR selective antagonists, the A_3AR selective agonists required more H-bonding ability, especially at the ribose position. This pharmacophore study is consistent with the *C* log *P* result; agonists are more hydrophilic in comparison to nonnucleoside antagonists. This also agreed with the A_3AR docking results (see below), which showed H-bonding to the ribose moiety of the agonist that was absent in docking of nonnucleoside antagonists in the right side of Fig. 3.

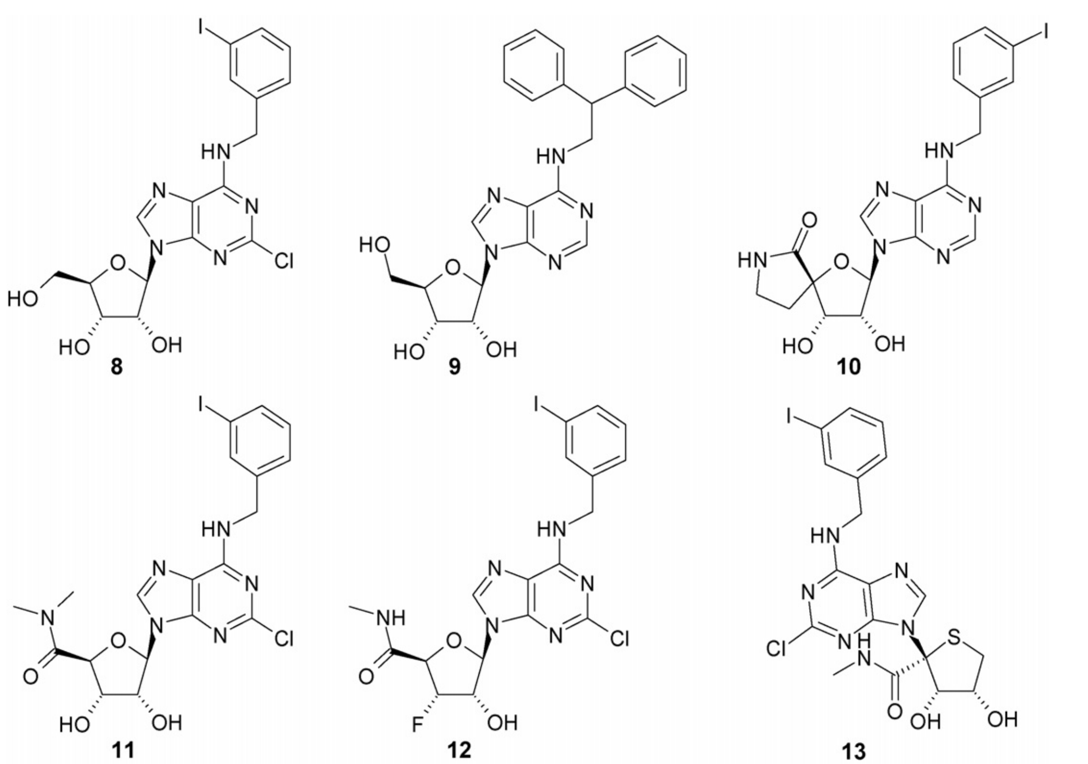

Chart 2. The structures of various nucleoside A_3AR antagonists. (**8**) MRS542, (**9**) MRS3310, (**10**) MRS1292, (**11**) MRS3771, (**12**) MRS3156, (**13**) MRS3057.

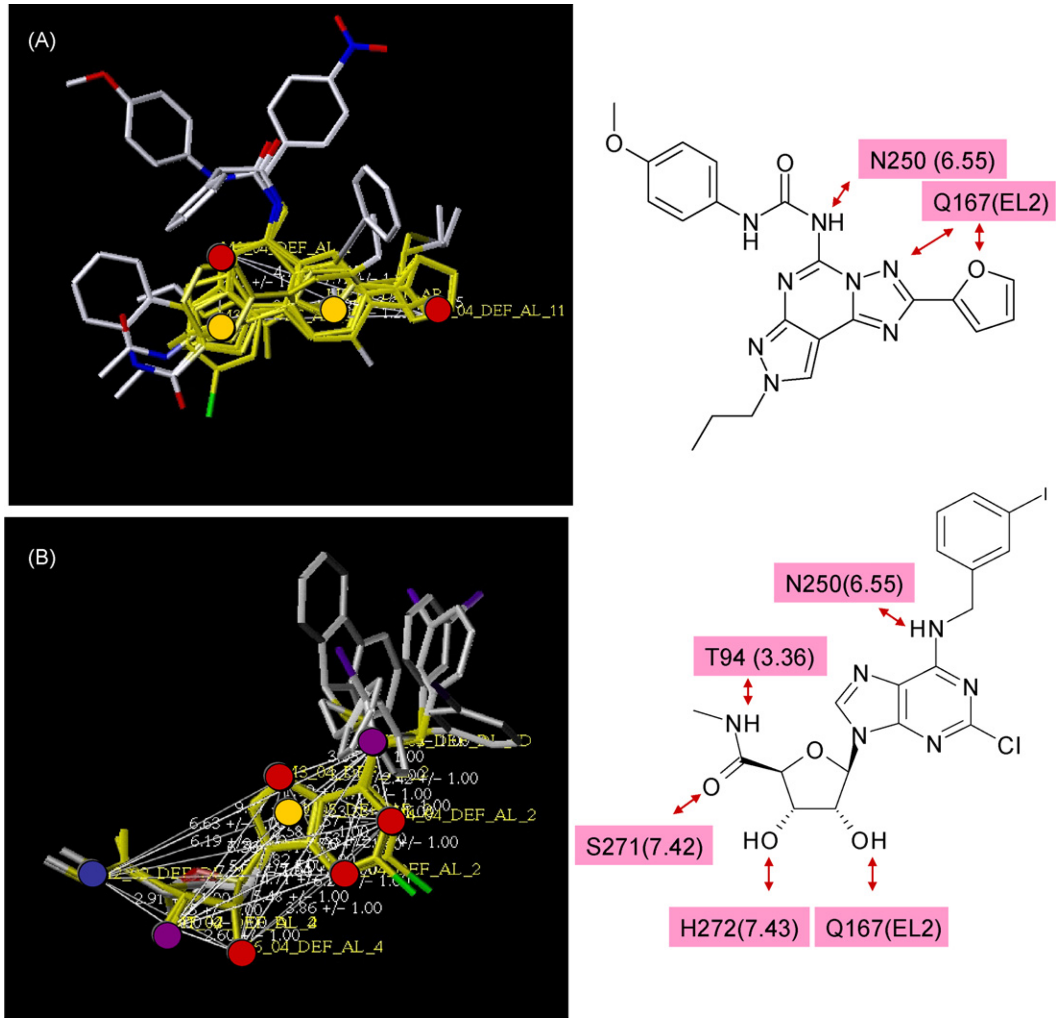

Fig. 3. Pharmacophore analysis of sets of A_3AR selective antagonists (A) and agonists (B) using a DISCO method (common pharmacophores shown on left side) and interactions of neutral antagonist **7** and full agonist **21** with specific amino acid residues derived from hA_3AR receptor docking (right side). The colored circles represent pharmacophoric elements common within each compound set: yellow for the center of aromatic ring, red for an H-bond acceptor, blue for an H-bond donor, purple for an H-bond donor or acceptor. Nucleoside antagonists were not included in this analysis.

2.4. *Conformational distinction of the A_3AR in resting and agonist-bound states*

If the receptor is assumed to exist simply in two functional conformational states, inactive or active, then a full agonist may prefer to bind at the active conformation with a local conformational change to subsequently undergo an overall conformational change upon activation. Because of the difficulty to generate a fully active conformation (e.g. Meta II of rhodopsin) for analyzing agonist binding, the binding preference of full agonists to the Meta I conformation and to the ground-state conformation was studied. Our docking studies of various A_3AR selective agonists and antagonists suggested that a major, characteristic outward movement of the conserved W6.48 in TM6 occurs upon the binding of a nucleoside agonist, but not a nucleoside or a nonnucleoside antagonist [12]. The importance of $W265^{6.48}$ in rhodopsin activation was suggested in a UV–visible spectroscopic analysis of site-directed mutagenesis of this residue. The differential absorbance indicated that perturbations in characteristics of $W126^{3.41}$ and $W265^{6.48}$ resulted from a general conformational change concomitant with Meta II formation [26]. There was a rearrangement close to the bend of TM6 upon Meta I formation. The electron density featured a significant deviation from the position of $W265^{6.48}$ in the ground-state structure, suggesting the possibility of movement of W6.48. Meta I formation involved no large rigid-body movements or rotations of helices from their position in the ground-state. Instead, changes seemed to be localized, probably involving movement of side-chains such as $W265^{6.48}$ in kinked regions of helices close to the retinal-binding pocket [15].

The antagonist showed preferential docking at an A_3AR conformation based on the X-ray structure of the resting state of rhodopsin, while the agonist showed preferential docking at a putative Meta I state conformation of the A_3AR. The putative Meta I state conformation was generated by modeling the rearrangement of the side-chain of W6.48, as described in Section 5. All of the nonnucleoside antagonists preferred to bind to the g+ conformer of W6.48, whereas agonists displayed the binding preference of the g− conformer. N^6-(*R*)-[2-(3,5-

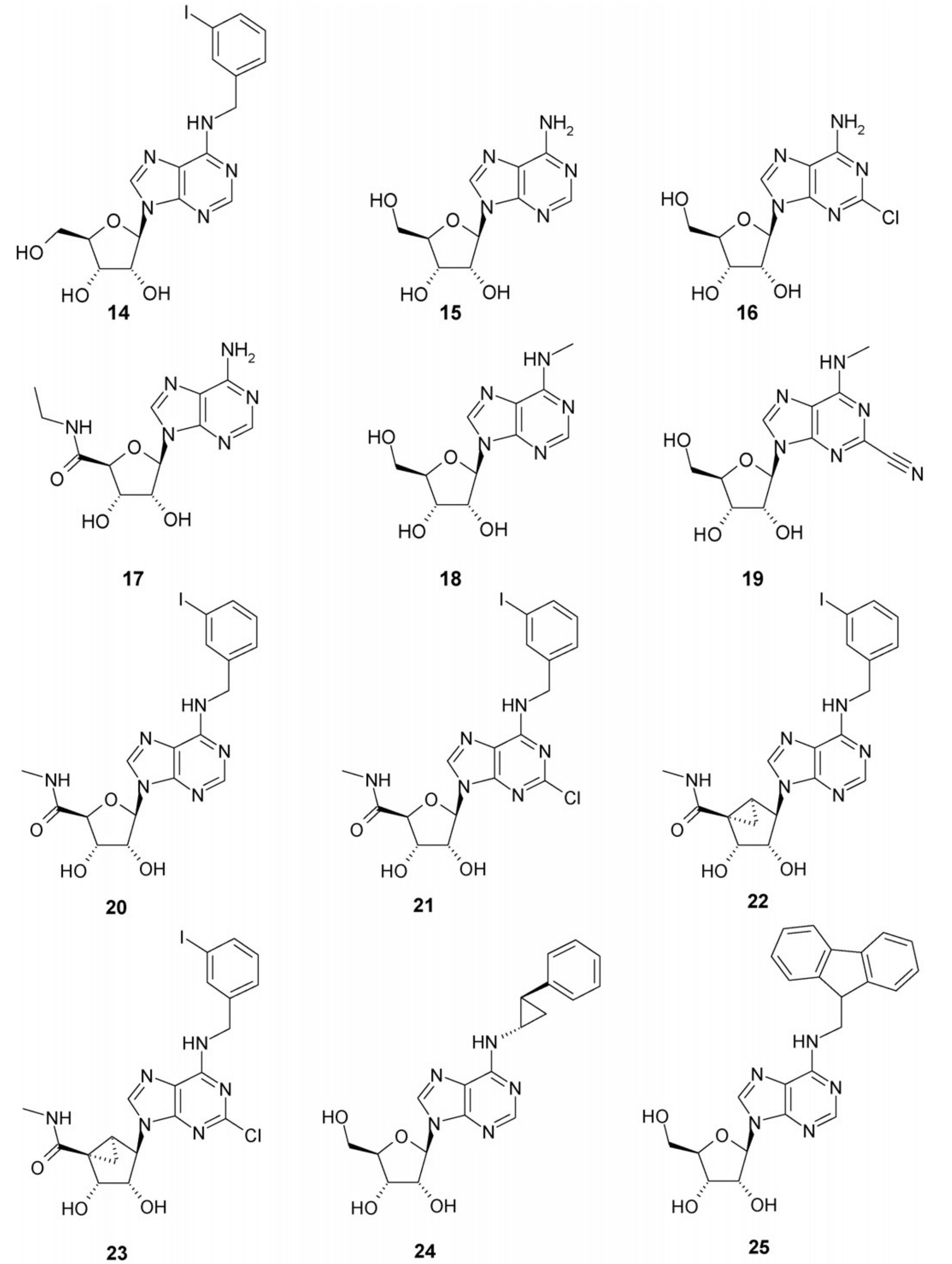

Chart 3. The structures of various nucleoside A_3AR ligands. (**14**) MRS541, (**15**) adenosine, (**16**) CADO, (**17**) NECA, (**18**) N^6-Me-adenosine, (**19**) MRS3244, (**20**) IB-MECA, (**21**) Cl-IB-MECA, (**22**) MRS1939, (**23**) MRS1898, (**24**) MRS3138, (**25**) MRS3279. Compound **14** is a partial agonist, and the remaining derivatives are full A_3AR agonists.

dimethoxyphenyl)-2-(2-methylphenyl)ethyl] adenosine, (*R*)-DPMA, activates with K_i values of 4.4 and 153 nM for the rat $A_{2A}AR$ ($rA_{2A}AR$) [27] and the $hA_{2A}AR$, respectively, whereas the same compound bound to the A_3AR with a K_i value of 106 nM, but with 0% efficacy. Similarly, N^6-(2,2-diphenylethyl)adenosine **9** acted as a full agonist at $rA_{2A}AR$ (K_i: 25 nM) but as an antagonist at hA_3AR (K_i: 3.9 nM). To study the binding preference of nucleoside antagonist and agonist, two different g conformers of W265$^{6.48}$, i.e. for the Meta I state conformation and for the ground-state conformation, were used. The docking result with two different conformations suggests that (*R*)-DPMA and **9** as $hA_{2A}AR$ agonists preferred to bind at the Meta I-like conformation of the $A_{2A}AR$. The total energy of each of their complexes was 7 kcal lower than that of the inactive state complex. While the same compounds as A_3AR antagonists, (*R*)-DPMA and **9**, exhibited a binding

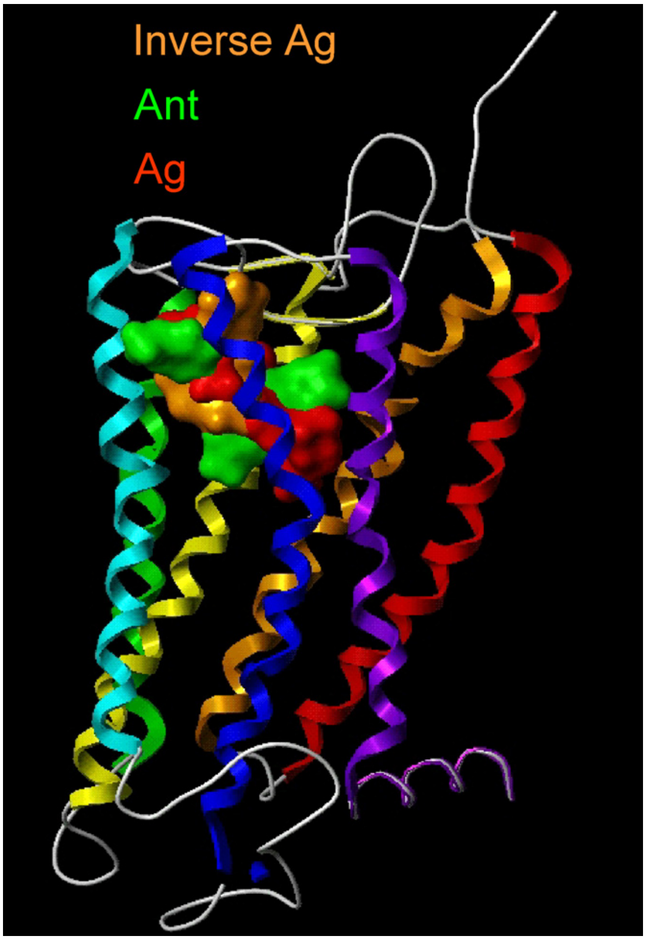

Fig. 4. The domains within the TM binding cavity of A_3AR for a representative inverse agonist **1** (orange), neutral antagonist **7** (green), and full agonist **21** (red). Using MOLCAD ribbon surface program, each ligand is represented by a Connolly surface model. The A_3AR is shown using a ribbon model with different colors for each TM (TM1: red, TM2: orange, TM3: yellow, TM4: green, TM5: cyan, TM6: blue, TM7: purple, and H8: violet).

preference to the ground-state conformation of A_3 resulting in 7 kcal lower energy of the complex. These observations conclude that the binding preferences of the full agonist reflect biologically relevant, ligand-induced conformational changes.

2.5. Distinct binding domains for representative agonist, nonnucleoside antagonist, and inverse agonist

As prototypical ligands, we used an A_3AR selective inverse agonist PSB-11 **1** ((*R*)-8-ethyl-4-methyl-2-phenyl-imidazo[2,1-i]purin-5-one, hA_3 $K_i = 2.3$ nM) [28], a neutral antagonist MRE-3008F20 **7** (5-[[(4-methoxyphenyl)amino]-carbonyl]amino-8-methyl-2-(2-furyl)pyrazolo[4,3-e]1,2,4-triazolo[1,5-c]pyrimidine, hA_3 $K_i = 0.2$ nM) [29] and a full agonist Cl-IB-MECA **21** (2-chloro-N^6-(3-iodobenzyl)-5′-*N*-methylcarboxamidoadenosine, hA_3 $K_i = 1.4$ nM), as shown in Charts 1 and 3. The putative binding sites of these three representative ligands were compared.

The putative agonist binding site of the A_3AR was located in the upper TM region near EL2, as deduced from point-mutational results and a docking study [14]. In the present study, **1** and **7** were docked to the A_3AR model based on the inactive state of rhodopsin, and these complexes were compared to our previous model of **21** docked to the Meta I-like template. These three A_3AR selective ligands were partially overlapped in their putative binding domains, as depicted in Fig. 4. There were common binding regions for the imidazole N^8-H of the 2-phenylimidazo[2,1-i]purin-5-one ring in **1** and the exocyclic amino groups of the [1,2,4]triazolo[1,5-c]pyrimidine ring in **7** and the 9H-purine ring in **21** through H-bonding to the side-chain of N250$^{6.55}$. In addition, the NH of the side-chain of Q167 in EL2 formed H-bonds with the N^9 atom of imidazo[2,1-o]purin-5-one ring in **1**, the O atom of the furan ring in **7**, and the N^3 atom of the adenine ring in **21**. Clearly, different additional interactions were evident for each ligand. In the case of the inverse agonist **1**, there was no binding at the upper TM7, but additional binding of the 2-phenyl ring at the upper TM6 was shown. Additional antagonist interactions occurred at the upper regions of TMs 5 and 6 with the additional N^5-phenyl ring and at the upper regions of TMs 6 and 7 with the 2-furan ring. In the agonist binding domains, additional interactions at the site of helical bending of TM6 in proximity to TM7 were present. Ribose 3′- and 5′-substituents H-bonded with the hydrophilic amino acids, T3.36, S7.42, and H7.43, and the terminal methyl group of the 5′-uronamide interacted with the hydrophobic side-chain of F6.44 in the conserved FxxxW motif. The differences in the preference of binding domains for the A_3AR selective inverse agonist **1**, neutral antagonist **7**, and full agonist **21**, suggest a spatially distinct role of each ligand in binding and activation processes.

Docking results of ligands with diverse function suggest that each ligand possesses specific interactions. Previously, rhodopsin-based homology modeling of ARs was guided mainly by mutagenesis; currently, docking is performed by more systematic computational methods. Fig. 5 displayed docking complexes of the several A_3AR ligands obtained using FlexiDock and FlexX.

2.5.1. Docking of inverse agonist

The docking result of the inverse agonist **1** (Fig. 5A) showed H-bonding of the N^1H, N^9, and 5-CO atoms of the imidazopurinone ring with N250$^{6.55}$, Q167 in EL2, S181$^{5.42}$, respectively. The ethyl group at the C8 position interacted with L90$^{3.32}$ through a lipophilic interaction. The *S*-form of **1**, having the same overall geometry but a different direction of the ethyl group, displayed unfavorable interaction with a total complex energy 1.6 kcal higher than that for the *R*-form. The experimental result that the *R*-form bound to the A_3AR with four-fold higher affinity than the *S*-form correlated with the docking result.

2.5.2. Docking of nucleoside antagonists

The flexibility of the 5′-uronamide group correlated with putative conformational changes of the receptor associated with the movement of W6.48 upon activation. As reported previously, the nucleoside antagonist **10** (K_i of hA_3: 29.3 nM, 0% efficacy), having reduced flexibility of the 5′-

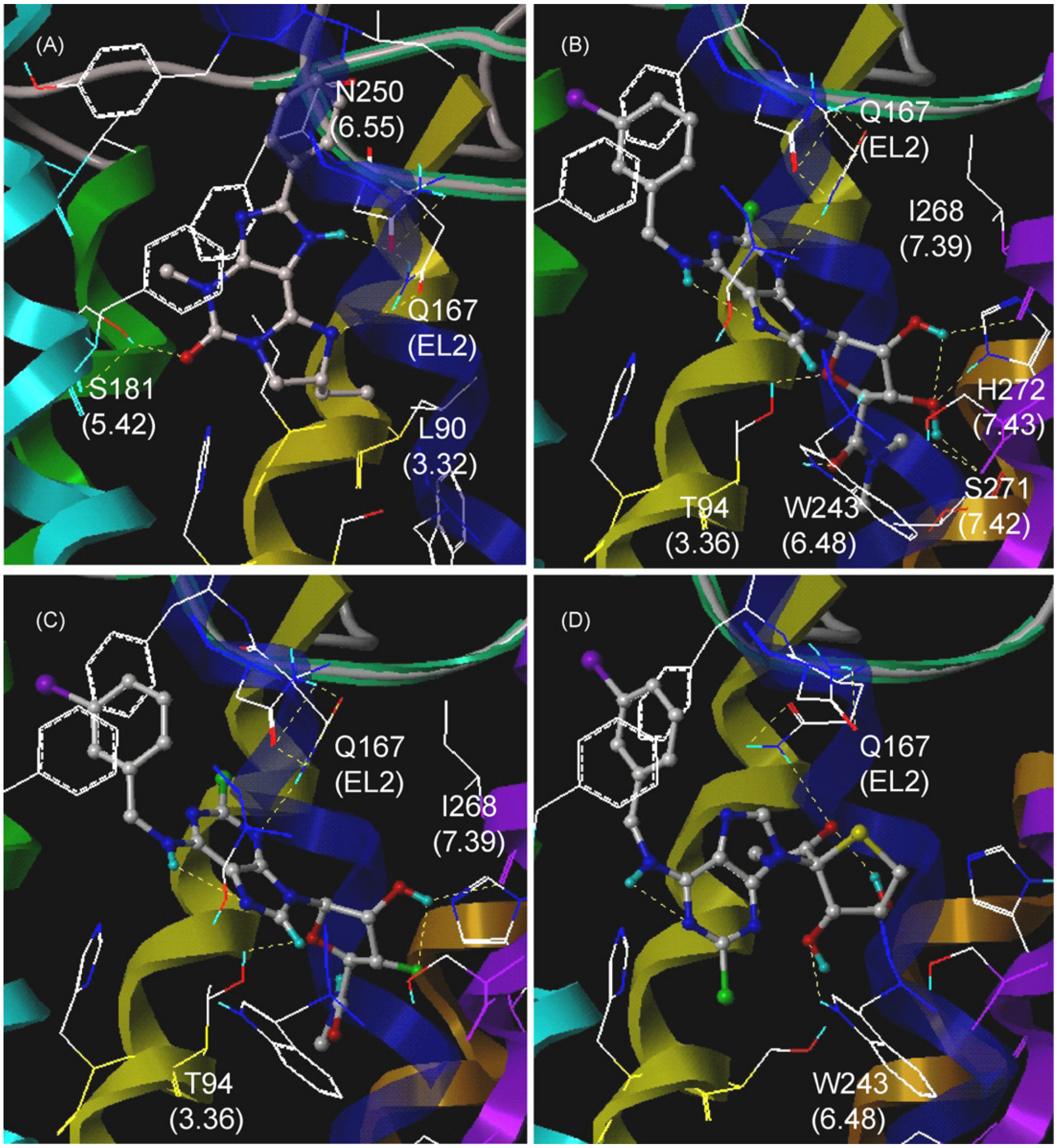

Fig. 5. Docking complexes of A_3AR antagonists. (A) **1**, the nonnucleoside (*R*)-PSB-11, (B) **11**, the 5′-*N*,*N*-dimethyluronamide MRS3771, (C) **12**, 3′-deoxy-3′-fluoro analogue MRS3156, (D) **13**, 4′-adenine analogue MRS3057. All ligands are represented by ball-and-stick models. Using MOLCAD ribbon surface program, the A_3AR are shown in ribbon model with different colors for each TM (TM1: red, TM2: orange, TM3: yellow, TM4: green, TM5: cyan, TM6: blue, TM7: purple, and H8: violet).

uronamide group, preferred to bind to the resting state. In addition, a recent study suggested that activation by an AR agonist also requires specific interactions at TMs 3 and 7, especially at T3.36, S7.42 and H7.43. Two selective A_3AR agonists, Cl-IB-MECA and its 4′-thio analogue, have been successfully transformed into antagonists selective for the A_3AR by appending an additional *N*-methyl group on the 5′-uronamide position [21]. The 5′-(*N*,*N*-dimethyl)uronamido group especially tends to preserve affinity and selectivity in N^6-3-iodobenzyladenosine derivatives, while entirely abolishing activation of the hA_3AR. As displayed in Fig. 5B, the docking result of compound **11** displayed orientations of CO and N atoms at the 5′-position similar to the previous docking result of compound **10**, resulting in the loss of H-bonding at $T94^{3.36}$ and $S271^{7.42}$. The 5′-uronamide group in Cl-IB-MECA with intramolecular H-bonding between 5′-NH and 4′-O, and between 5′-CO and 3′-OH in an energetically favorable conformer as well as a receptor-bound conformation interacted with the specific residues at TMs 3 and 7. However the 5′-cyclized uronamide in **10** and 5′-*N*,*N*-dimethyl uronamide in **11** did not adopt the receptor-bound agonist conformation because of a locked conformation and a different energetically favored geometry, respectively. The 5′-CO group in **10** and **11**, oriented perpendicular to the ribose ring, could form an H-bond with W6.48, thus blocking the shift of W6.48 side-chain during the conformational change.

The docking complex of compound **12** in Fig. 5C indicated the importance of TM7 binding for agonism. Compound **12**, the 3′-deoxy-3′-F analogue of Cl-IBMECA, bound to the A_3AR with a moderately decreased binding affinity but did not induce activation. The docking result showed a loss of the typical interaction of the nucleoside 3′-position with H7.42.

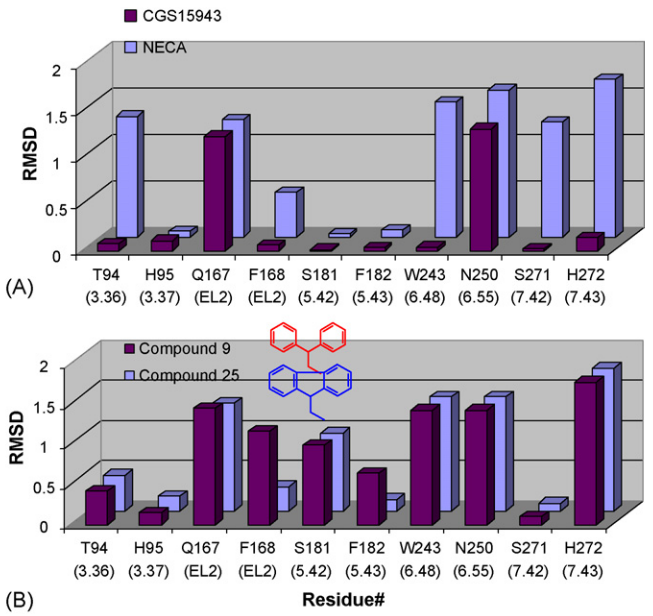

Fig. 6. RMSD values of the side-chains in binding domains between the ground-state without ligand and the bound-state after ligand binding. (A) Nonnucleoside antagonist CGS15943 and agonist NECA; (B) nucleoside antagonist **9** and the structurally related agonist **25**. All atoms excluding H atoms in the side-chains were included in the calculations.

The docking result of compound **13** (K_i of hA_3: 4.3 nM, 0% efficacy) in Fig. 5D displayed direct H-bonding of the side-chain of W6.48 with the 3′-OH group. The O atom of the 5′-CO group interacted additionally by H-bonding with Q162 in EL2. There were no interactions at T3.36, S7.42 and H7.43. The N^6-3-I-benzyl moiety formed a hydrophobic interaction with F168 in EL2 similar to other N^6-benzyl adenosine derivatives, while the binding site of the adenine ring was distinct from that of other nucleoside ligands or of nucleoside agonists.

2.6. RMSD analysis of conformational changes in amino acid side-chains

The conserved W6.48 and H7.43 residues in the ARs are important to constrain the inactive structure. In the ground-state structure, the highly conserved H7.43 formed an H-bond with the highly conserved E1.39. W6.48 was also important for an intramolecular TM network through hydrophobic as well as hydrogen-bonding interactions. Thus, agonist binding and activation disrupts the ground-state intramolecular TM networks and thus destabilizes these structural constraints. An interaction of the ribose moiety at T3.36 and S7.42 also facilitates conformational change.

This docking study was consistent with a study of the root mean square deviation (RMSD) of several side-chains in the binding domains when the RMSD value was checked between the ground-state and the bound-state of the A_3AR upon binding of the 1H-[1,2,4]triazolo[1,5-c]quinazoline derivative, CGS15943, as a non-selective antagonist, and NECA **17**, as a full agonist. A high RMSD, shown at the side-chains of $Q167^{EL2}$ and $N250^{6.55}$, was common to binding of both agonist and antagonist (Fig. 6A). A clear difference upon nucleoside agonist binding was responsible for the additional high RMSD values at T3.36, W6.48, and S7.42 and H7.43 in comparison to nonnucleoside antagonist binding. Thus, activation appears to require specific conformational changes associated with the rearrangement of particular residues. TM3 and the upper portions of TMs 6 and 7 near the kink site seem to be especially important for these conformational changes.

In the case of adenosine derivatives having a 5′-OH group, changes in the binding site of large N^6-groups at the upper regions of TMs 4 and 5 also appear to be correlated with A_3AR activation. Relatively bulky cyclic aliphatic rings at the N^6-position tended to reduce the efficacy as well as the binding affinity at the hA_3AR. For example, the relative efficacy was 100% (K_i of hA_3: 6.4 nM), 97% (K_i of hA_3: 72 nM), 76% (K_i of hA_3: 73 nM), and 49% (K_i of hA_3: 411 nM) for the N^6-cyclobutyl, the N^6-cyclopentyl, the N^6-cyclohexyl, and the N^6-cyclooctyl-substituted derivatives of adenosine, respectively. The flexible N^6-(2-phenylethyl) adenosine decreased the A_3AR efficacy to 84%, whereas its conformationally constrained analogue **24** through the introduction of the cyclopropyl ring at the N^6-position was a full agonist.

To study the optimum binding domains of the phenyl ring of N^6-2-phenylethyl adenosine, six different conformations were generated by rotating the t_1 torsion angle (N^6-C-C-C_{ar}) by 60° increments and compared in thermal stability at the N^6-binding domains. A major difference was shown in relation to the two side-chains of the Phe residues, $F168^{EL2}$ and $F182^{5.43}$, although both nucleoside agonists and antagonists with a 5′-OH group displayed no binding difference at the ribose-binding region. The most energetically favorable conformer of the N^6-(1S, 2R)-2-phenylcyclopropyl analogue **24**, which was also the highest energy conformer of the N^6-2-phenylethyl adenosine, displayed a t_1 angle of +140°. While its regioisomer N^6-(1*R*,2*S*)-2-phenylcyclopropyl adenosine with 87% efficacy exhibited a favorable t_1 angle of −140°, corresponding to the energetically favorable conformer of the N^6-2-phenylethyl adenosine. It required an outward rotation of the $F182^{5.43}$ side-chain. This result was consistent with the RMSDs determined within the binding domains after docking of a nucleoside antagonist and agonist. The analysis of RMSDs comparing the receptor complexes with docked antagonist **9** and agonist **25** indicated that the binding of the flexible N^6-(2,2-diphenylethyl) adenosine **9** resulted in a high RMSD with respect to binding at $F168^{EL2}$ and $F182^{5.43}$ but similarly high RMSDs at T3.36, W6.48, and H7.43 in Fig. 6B. However, the RMSDs of the complex of the conformationally constrained N^6-fluorenyl-methyl derivative **25** tended to be low. In the case of compound **9**, the binding of one phenyl ring, which protruded toward TMs 5 and 6, required the outward rotation of $F182^{5.43}$ in Fig. 7. The position of the phenyl ring was related to the movement of $F168^{EL2}$ and $F182^{5.43}$. Thus, unlike binding at TMs 6 and 7, antagonist binding but not agonist binding might require the disruption of the side-chain at the N^6 binding domain. Our previous experiments indicated the F182A mutations eliminated the effects of three heterocyclic allosteric modulators of the A_3AR (DU124183, VUF5455, HMA) and of sodium ions,

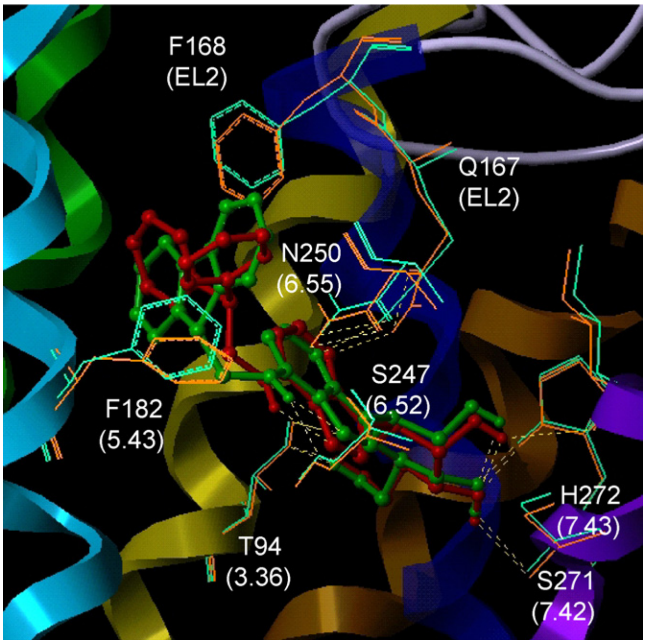

Fig. 7. Superimposition of the N^6-aralkyl adenosine agonist **25** in green and closely related antagonist **9** in red. All ligands are represented by ball-and-stick models. The side-chains in the binding site were colored in blue for agonist binding and in orange for antagonist binding. The A_3AR is shown as a tube model with different colors for each TM (TM1: red, TM2: orange, TM3: yellow, TM4: green, TM5: cyan, TM6: blue, TM7: purple, and H8: violet).

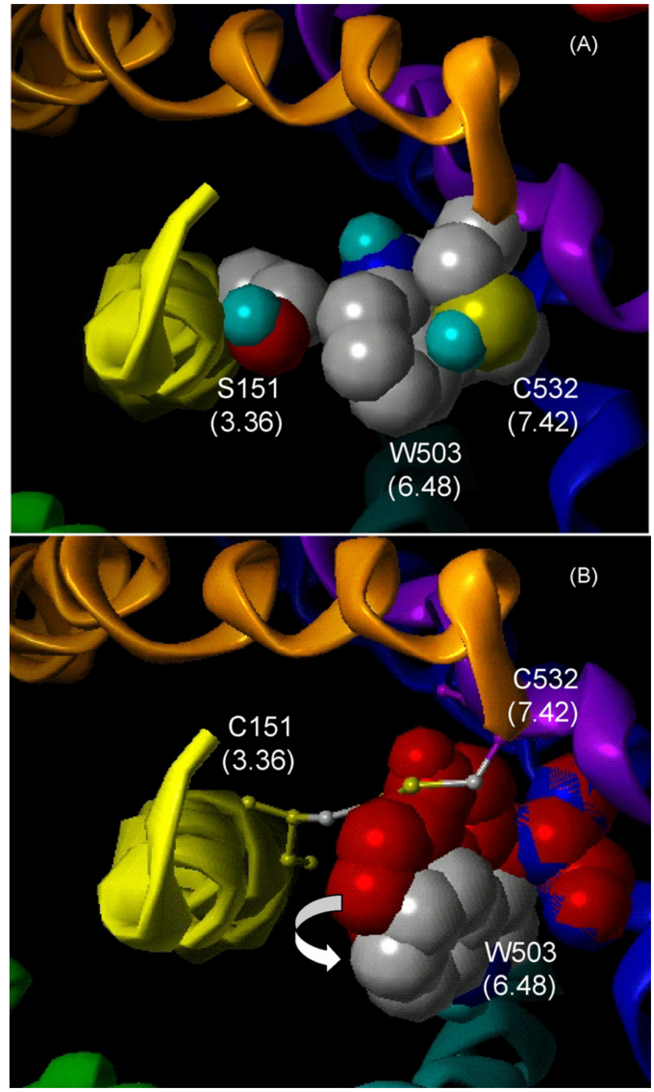

Fig. 8. The 3D model of the rat M_3 muscarinic receptor and its internally crosslinked S151C mutant receptor. (A) The residues S3.36, W6.48, and C7.42, are shown in space-filling model viewed from the extracellular side, (B) In the same view of (A), the result of 1 ns MD of the M_3 S151C mutant receptor displayed a reduced distance from 8.2 to 6.6 Å between the two α-carbon atoms of C151 and C532, which formed a disulfide bond. In addition, the side-chain of W6.48 (red) from the inactive state required the outward movement (white), indicated by the arrow. The M_3 muscarinic receptor is shown as a tube model with different colors for each TM (TM1: red, TM2: orange, TM3: yellow, TM4: green, TM5: cyan, TM6: blue, TM7: purple, and H8: violet).

which modulate agonist binding [30]. The atomic force microscopy dimer model of mouse rhodopsin defined the dimer interface as the face of TMs 4 and 5 [31]. A conformational change, such as a rearrangement of the dimer interface, is proposed as a critical component of the GPCR activation mechanism [32]. Recent data support an important role of $F182^{5.43}$ in activation [30], especially in signal amplification through domain–domain interaction. $F182^{5.43}$ seems to be structurally important for the dimerization interface and for activation.

2.7. Proposed activation mechanism

Although there is no global active state model, local conformational changes upon activation have been proposed. We previously obtained evidence in docking studies for a movement of TM6 upon agonist activation. The agonists containing a 5′-alkyluronamide group, which restores full efficacy in the A_3AR, interacted through additional H-bonding with the hydrophilic amino acids, T3.36 and S7.42, and hydrophobic interactions of the terminal methyl group of the 5′-uronamide with the hydrophobic side-chain of F6.44 in the FxxxW region. The low efficacy of 5′-thioether derivatives [20] is consistent with the need for H-bonding in this region in order to activate the A_3AR. Rhodopsin activation also correlated with the requirement of upper TM6 movement at the beginning of activation. Other binding requirements for A_3AR activation include the interaction at H7.43 with the 3′-hydroxyl group. These specific interactions at the kink site required the characteristic outward side-chain movements of TMs 3, 6 and 7 in the anti-clockwise direction from the extracellular view. The docking study of the antagonist N^6-(2,2-diphenylethyl)adenosine **9** suggested a small clockwise outward rotation of the $F182^{5.43}$ side-chain, as viewed from the extracellular side, in antagonist binding but not in agonist binding. A_3AR activation appears to involve an opposite movement, i.e. an anti-clockwise inward rotation of TM5. This prediction correlated with the activation of the M_3 muscarinic acetylcholine receptor from a study of *in situ* disulfide cross-linking at the cytoplasmic ends of TMs 5 and 6. The study with the rhodopsin-based model predicts an outward movement and/or a clockwise rotation of both TMs 5 and 6, as viewed from the cytosolic side [33].

Results of a parallel study of the rat M_3 muscarinic receptor were consistent with our docking result of the A_3AR agonist with respect to movement of upper TMs 3 and 7. A study of *in situ* disulfide cross-linking [34] between the TMs indicated that agonists but not antagonists promoted the formation of a disulfide bond between $S151C^{3.36}$ and an endogenous $C532^{7.42}$. Their corresponding amino acids are T3.36 and S7.42, which are involved only in agonist binding in the A_3AR. A 3D model indicated that $C532^{7.42}$ and $S151^{3.36}$ faced each other in the center of the TM receptor core, showing a 8.2 Å distance between the two α-carbon atoms. Cross-linking indicated that the two residues were separated by a distance between α-carbon atoms of ~10 Å. However, in the ground-state structure of the M_3 muscarinic homology model (PDB ID: 2AMK), W6.48 interfered in the contact between these helices. As displayed in Fig. 8A, the side-chain of W6.48 was located in the middle of the two side-chains, $S151C^{3.36}$ and $C532^{7.42}$. In the resting state, it appeared to interfere with the formation of a disulfide bond between these Cys residues. The W6.48 also constrained the inactive state conformation through an intramolecular TM H-bonding network as well as a hydrophobic interaction, as displayed in the A_3AR. Constrained 1 ns MD of the ligand complex with the S151C mutant receptor displayed a reduced distance between TMs 3 and 7. The distance between the two α-carbon atoms was reduced from 8.2 to 6.6 Å. In addition, the side-chain of W6.48 displayed an outward rotation in Fig. 8B. Assuming a conserved activation mechanism of Family A GPCRs, a large movement of upper TM6 is followed by a slight movement of TMs 3, 5, and 7, each moving in an anti-clockwise direction from the extracellular side.

3. Discussion

All GPCRs have common structural components, including seven TM-spanning α-helical segments connected by alternating intracellular and extracellular loops (ELs), with the amino terminus on the extracellular side and the carboxyl terminus on the intracellular side. Although the overall sequence homology among all Family A receptors is less than 20%, sequence analysis suggested that Family A GPCRs could share the same arrangement of the seven helices in the plane of lipid bilayers, because of the presence of a few highly conserved residues and motifs in each of the seven helices. The most conserved amino acids, in the range of 80–100% from a recent study on the alignment of 270 members of Family A, are N1.50, L2.46, D2.50, C3.25, E/D3.49, R3.50, W4.50, P5.50, F6.44, W/F6.48, P6.50, P7.50, and Y7.53 [35]. The study of homology models showed that those highly conserved residues are involved in an intramolecular TM H-bonding network, as well as in characteristic folding [14]. The highly conserved residue D2.50 formed an intramolecular TM network though H-bonding with several residues in (N7.45, S7.46, N7.49) in TM7, which was also associated with TMs 3 (S3.39) and 6 (W6.48). The highly conserved N1.50 is in proximity to D2.50. The highly conserved R3.50 in the DRY motif also interacted with the conserved E6.30 in TM6 through a salt bridge. The conserved W4.50 formed an H-bond with the conserved S2.45 in TM2. The residues H7.43 and E1.19, both conserved in ARs, were associated through H-bonding. The highly conserved P residues in TMs 5, 6, and 7 displayed a characteristic kink in each helix. The disulfide bond between C3.25 and another Cys residue of the second extracellular loop (EL2), which is 90% conserved, points to potential similarities in EL2 within Family A. The highly conserved motifs at the upper TM region of FxxxW in TM6, with frequencies of 89 and 90% for Phe and Trp, and the cytosolic side of E/DRY in TM3 and $NPxxY(x)_{5,6}F$ in TM7 suggest a conserved mechanism of activation and signal transduction, while the ligand binding site is the least conserved in order to accommodate the diversity of ligands.

Site-directed mutagenesis and molecular modeling have revealed that the inactive state conformations are stabilized by specific intrahelical salt bridge interactions, H-bonding and hydrophobic interactions. Ordered water molecules extended the hydrogen bonding network, linking $W265^{6.48}$ in the retinal-binding pocket of bovine rhodopsin to the NPxxY motif near the cytoplasmic boundary, and the E113 (3.28) counterion of the protonated Schiff base to the extracellular surface [36]. The activation of GPCRs is generally assumed to result in a significant structural rearrangement of the receptor, presumably involving the rigid-body movement of TMs. Constitutively activating mutations or agonist binding disrupts such constraining interactions leading to a receptor conformation that associates with and activates a G-protein.

There was a higher degree of conservation in the lower part of the GPCRs near the cytoplasmic domain, indicating a conserved mechanism of activation and signal transduction. When various ligands bound to the least conserved binding site distant from the site of G-protein regulation, the structural changes leading to Meta II are believed to be similar to the activation steps of Family A GPCRs. Rhodopsin structural studies propose that activation by light opens a cleft at the cytoplasmic end of the helix bundle, with (1) separation of TMs 3 and 6, (2) increased exposure of the inner faces of TMs 2, 3, 6, and 7, and (3) decreased exposure near the ends of TMs 4 and 5 [10]. The study of the environmentally sensitive and cysteine-reactive fluorescent probe IANBD monitored agonist-induced structural changes and predicted conformational changes accompanying activation of the β_2-adrenergic receptor [37]. It was concluded that an agonist-induced rigid-body movement of TM3 and 6 occurs as an anticlockwise rotation from the extracellular perspective. These observed changes in fluorescence were consistent with spin-labeling studies in rhodopsin. The observed pattern of *in situ* disulfide cross-links with modeling studies of the M_3 muscarinic receptors led to several predictions: (1) M_3 receptor activation induced a major rotational movement of TM7 [38,39], (2) structural changes allowed the cytoplasmic ends of TMs 5 and 6 to move toward each other [33], and (3) the agonist binding site upon activation pulled the exofacial segments of TMs 3 and 7 closer together during the early conformational events [39]. Several theoretical active structures of rhodopsin, based on the various experimental results [8,9], indicated that common predicted conformational changes were the large movement of upper

TM6 and other smaller changes at TMs 3, 4, 5, and 7, although the overall structures are different. Thus, the agonist-induced conformational changes leading to G-protein activation for rhodopsin-like Family A GPCRs appear to be similar to those observed for rhodopsin. Cumulative experimental data conclude that TMs 3, 6, and 7 are mainly involved in the activation of GPCRs.

To describe the process of agonist activation of GPCRs, several kinetics models have been developed [40]. In the simplified model, a ligand induces a conformational change in the receptor, thereby conferring affinity of the receptor for the next signaling protein in the transduction cascade (e.g. a G-protein). The intensity of the stimulus may be related to the degree of change in conformation, the frequency of change in conformation, or the duration of the induced conformation. A two-state model has suggested that a receptor exists primarily in two conformations, an inactive state (R) and an active state (R^*) [40]. In the absence of agonist, the active state occurs with a constitutive activation. Hence, by different binding preferences the agonist or the inverse agonist either increases or decreases, respectively, the population of these conformations (R^*), to produce a functional response; full agonists stabilize R^*, whereas inverse agonists stabilize R [41].

The A_3AR was selected as a model system to study the activation mechanism of rhodopsin Family A GPCRs. We analyzed the molecular properties, the pharmacophore differences, the structural requirements, and the binding preference between antagonist and agonist. The molecular modeling result clearly indicated that the relative efficacy of ligands depends on characteristic functional groups and their specific binding domains. The distinct binding sites of different functions of ligands might influence differently the conformational change occurring upon activation. We could differentiate the characteristics of agonist and antagonist through the calculation of molecular properties and the study of pharmacophore models: agonists are more hydrophilic and include more H-bonding groups in ribose region compared to antagonists.

Our current models of the mechanism of GPCR activation by diffusible agonists have been deduced from indirect docking studies of the binding domain. These indirect docking studies provide only limited insight into the agonist-induced structural changes that define the active state of the receptor. However, a significant distinction between the docking result of agonists and antagonists was whether agonist additional binding of the ribose group in the FxxxW domain could affect the movement of W6.48 and H7.42, which formed an important H-bonding TM network in the ground-state structure. The binding character at the 3′- and 5′-positions of the ribose ring correlated with the specific interactions at T3.36, S7.42, and H7.43, which displayed major disruption upon agonist binding with high RMSD values. The mode of agonist binding to TMs 3, 6, and 7, which are highly conserved within ARs, suggests a possible conserved activation mechanism for all of the ARs. The N^6 binding region, which was located at upper TMs 4 and 5 including EL2, known to form the dimerization interface, also regulated the A_3AR activation. The binding preference of nucleoside agonists clearly exhibited a preference for the theoretically generated Meta I state conformation and the rearrangement of W6.48 through an anti-clockwise rotation from the extracellular perspective.

Each compound differs in the function as well as in the binding affinity at different subtypes of ARs. The same compounds bind with various binding affinities and function as agonists or antagonists depending on the subtype. (R)-DPMA, a potent agonist for the $rA_{2A}AR$ (K_i: 4 nM), was demonstrated to be a moderately potent antagonist for the hA_3AR (K_i: 106 nM). The binding affinity can be explained using each drug-receptor molecular pair, but the ligand function through activation or inactivation, drug efficacy, cannot be considered simply as single receptor versus single ligand property. In addition, agonist binding to the A_3AR has been shown to be always totally entropy-driven, while antagonist binding was enthalpy- and entropy-driven [42]. This thermodynamic discrimination of agonists from antagonists might require flexibility at the 5′-position of the ribose ring for agonism. The broad distribution of the short lifetime components in the fluorescence lifetime analysis of the β_2-adrenergic receptor suggests there is considerable flexibility in the agonist-induced conformation [40]. The study represents agonists stabilizing a series of agonist-specific active states, indicating functional differences between agonists and partial agonists. Current agonist docking complexes may represent only a single snapshot of possible multiple active conformations that could be stabilized by drugs.

The increasing evidence that virtually all GPCRs form oligomeric complexes *in vivo* should compound the level of complexity in the drug development process. The drug efficacy as a function of the entire GPCR system, involving both the receptor and its cellular environment (G-protein, GPCRs, water, lipid bilayer, etc.) will need to be taken into consideration in the development of new therapeutic agents in the future.

4. Conclusions

The molecular modeling results clearly delineated the interactions involved in the binding of agonists and antagonists, which correlated well with known experimental results. The calculation of molecular properties and the study of pharmacophores indicated the characteristic differences between agonists and antagonists. The docking complexes provided insight into the conformational and binding requirements for agonists and antagonists at the A_3AR. Combination of the docking studies and pharmacophore analysis was helpful to understand the molecular mechanisms of receptor activation. The common requirements for A_3AR activation include: the destabilization of H-bond networks at W6.48 and H7.43, the specific interactions at T3.36, S7.42, and H7.43, the stabilization or the inward movement of F5.43, and the characteristic rotation of W6.48 to induce receptor activation. The results are consistent with the anti-clockwise rotation of TMs 3, 5, 6, and 7 from the extracellular view from other experimental results with Family A GPCRs. Thus, our findings suggest that the conformational changes associated with A_3AR activation are similar to those in rhodopsin and indicate a shared mechanism of GPCR activation.

5. Computational methods

5.1. Molecular modeling

All calculations were performed on a Silicon Graphics (Mountain View, CA) Octane workstation (300 MHz MIPS R12000 (IP30) processor). All ligand structures were constructed with the use of the Sketch Molecule of SYBYL 7.0 [43].

5.2. The 3D-structure and pharmacophore analysis of ligands

A conformational search of each ligand was performed by random search of flexible bonds. The low-energy conformers from the random search were re-optimized, removing all constraints. The options of random search for all rotatable bonds were 3000 iterations, 3-kcal energy cutoffs, and chirality checking. In all cases, MMFF force field [44] and charge were applied with the use of distance-dependent dielectric constants and conjugate gradient method until the gradient reached 0.05 kcal mol^{-1} $Å^{-1}$. After clustering the low-energy conformers from the result of the conformational search, the representative ones from all groups were reoptimized by semiempirical molecular orbital calculations with the PM3 method in the MOPAC 6.0 package [45]. The $\log P$ of each ligand was predicted by $C \log P$ calculation. Each of the common bioactive conformations from the conformer libraries was used for DISCO (DIStance COmparisons) computation [46] with the default option. Pharmacophore elements include hydrogen bond donor atoms, hydrogen bond acceptor atoms, and centers of mass of hydrophobic rings.

5.3. The generation of a putative Meta I state conformation of the A_3AR

The stabilities of three different χ_1 angles of W265$^{6.48}$ set at 60°, 180°, and −60° were compared. A minimized gauche + (g+) conformation with a χ_1 angle of −98° in the ground-state had the lowest energy among three different geometries. A gauche− (g−) conformer of W265$^{6.48}$ with the highest energy seemed to be similar to the Meta I state conformation, because it displayed the most outward anti-clockwise rotation from the extracellular view, as both rhodopsin studies and current agonist docking suggested. This putative Meta I state was used for agonist docking.

5.4. Induced-fit docking study

The homology model of the $hA_{2A}AR$ (PDB id: 1UPE) and the hA_3AR (PDB id: 1OEA) using the X-ray structure of bovine rhodopsin with a 2.8 Å resolution (PDB id: 1F88) as a template were used for the docking study. The A_3AR conformations based on the X-ray structure of the resting state of rhodopsin and the putative Meta I state were used for antagonist docking and for agonist docking, respectively. For induced-fit docking study, automatic flexible docking methods facilitated through the FlexX and FlexiDock utilities in the Biopolymer module of SYBYL v7.0 were used. FlexX 1.13 [47] is a fast docking method that uses a new algorithmic approach based on a pattern recognition technique called pose clustering, allowing conformational flexibility of the ligand according to a MINUMBA [48] conformer library to grow ligands during the docking process. The free binding energy of the complex including H-bond, ionic, aromatic, or lipophilic interactions, was estimated by the scoring function. Cscore calculations were included for scoring. To generate a set of reasonably docked ligands, the receptor description file (RDF) was generated to describe the binding site and specific torsion angles of important residues for ligand binding. In RDF file, a putative binding site including T94$^{3.36}$, N250$^{6.55}$, S271$^{7.42}$, and H272$^{7.43}$ was manually selected, based on the previous point-mutational results [30]. Formal charges were applied to the ligands. All default parameters, as implemented in the 7.0 release of SYBYL, were used. During flexible docking, only the ligand was defined with rotatable bonds. From the 30 docked structures, several starting positions of the ligand were selected for further FlexiDock steps. After the hydrogen atoms were added to the receptor, atomic charges were recalculated by using Kollman All-atom for the protein and Gasteiger-Hückel for the ligand. H-bonding sites were marked for all residues in the active site and for ligands that were able to act as H-bond donor or acceptor. Several pre-positioned ligands from the FlexX result were used as a starting point for FlexiDock. Default FlexiDock parameters were set at 3000-generation for genetic algorithms. To increase the binding interaction, the flexibility of both receptor and ligand was considered. The torsion angles of the side-chains that directly interacted within 5 Å of the ligands (T94$^{3.36}$, N250$^{6.55}$, S271$^{7.42}$, and H272$^{7.43}$) as well as various ligands, were selected as rotatable bonds. Finally, the complex structure was minimized by using an Amber 7 force field 99 with a fixed dielectric constant (4.0), until the conjugate gradient reached 0.1 kcal mol^{-1} $Å^{-1}$.

5.5. MD of rat M_3 muscarinic receptors

For the conformational refinement of the S151C mutant receptors, the optimized structures were then used as the starting point for subsequent 1-ns MD, during which the protein backbone atoms in the secondary structures were constrained as in the previous step. The options of MD at 300 K with a 0.2-ps coupling constant were a time step of 2 fs and a nonbonded update every 25 fs through the MD program in the SYBYL v7.0. The lengths of bonds with hydrogen atoms were constrained according to the SHAKE algorithm [49]. The average structure from the last 100-ps trajectory of MD was re-minimized with backbone constraints in the secondary structure and then without all constraints as described above.

Acknowledgements

This research was supported by the Intramural Research Program of the NIH, National Institute of Diabetes and Digestive and Kidney Diseases. We thank Dr. Jürgen Wess (NIDDK) for helpful discussions.

References

[1] K.A. Jacobson, Z.G. Gao, Adenosine receptors as therapeutic targets, Nature Rev. Drug Disc. 5 (2006) 247–264.

[2] L. Madi, S. Bar-Yehuda, F. Barer, E. Ardon, A. Ochaion, P. Fishman, A_3 adenosine receptor activation in melanoma cells: association between receptor fate and tumor growth inhibition, J. Biol. Chem. 278 (2003) 42121–42130.

[3] B.V. Joshi, K.A. Jacobson, Purine derivatives as ligands for A_3 adenosine receptors, Curr. Top Med. Chem. 5 (2005) 1275–1295.

[4] L. Yan, J.C. Burbiel, A. Maass, C.E. Müller, Adenosine receptor agonist: from basic medicinal chemistry to clinical development, Expert Opin. Emerg. Drugs 8 (2003) 537–576.

[5] Pharmaceutical R&D Benchmarking Forum, General Metrics, 2001.

[6] K. Palcezewski, T. Kumasaka, T. Hori, C.A. Behnke, H. Motoshima, B.A. Fox, I. Le Trong, D.C. Teller, T. Okada, R.E. Stenkamp, M. Yamamoto, M. Miyano, Crystal structure of rhodopsin: a G protein-coupled receptor, Science 289 (2000) 739–745.

[7] J.A. Ballesteros, L. Shi, J.A. Javitch, Structural mimicry in G protein-coupled receptors: implications of the high-resolution structure of rhodopsin for structure-function analysis of rhodopsin-like receptors, Mol. Pharmacol. 60 (2001) 1–19.

[8] G.V. Nikiforovich, G.R. Marshall, Three-dimensional model for Meta-II rhodopsin, an activated G-protein-coupled receptor, Biochemistry 42 (2003) 9110–9120.

[9] P.R. Gouldson, N.J. Kidley, R.P. Bywater, G. Psaroudakis, H.D. Brooks, C. Diaz, D. Shire, C.A. Reynolds, Toward the active conformations of rhodopsin and the β_2-adrenergic receptor, Proteins 56 (2004) 67–84.

[10] E.C. Meng, H.R. Bourne, Receptor activation: what does the rhodopsin structure tell us? Trends Pharmacol. Sci. 22 (2001) 587–593.

[11] G. Swaminath, Y. Xiang, T.W. Lee, J. Steenhuis, C. Parnot, B.K. Kobilka, Sequential binding of agonists to the β_2 adrenoceptor, J. Biol. Chem. 279 (2004) 686–691.

[12] Z.-G. Gao, S.-K. Kim, T. Biadatti, W. Chen, K. Lee, D. Barak, S.G. Kim, C.R. Johnson, K.A. Jacobson, Structural determinants of A_3 adenosine receptor activation: nucleoside ligands at the agonist/antagonist boundary, J. Med. Chem. 45 (2002) 4471–4484.

[13] K.A. Jacobson, Z.-G. Gao, S. Tchilibon, H.T. Duong, B.V. Joshi, D. Sonin, B.T. Liang, Semiempirical design of (North)-methanocarba nucelosides as dual acting A_1 and A_3 adenosine receptor agonists: novel prototypes for cardioprotection, J. Med. Chem. 48 (2005) 8103–8107.

[14] S.-K. Kim, Z.-G. Gao, P. van Rompaey, A.S. Gross, A. Chen, S. van Calenbergh, K.A. Jacobson, Modeling the adenosine receptors: comparison of the binding domains of A_{2A} agonists and antagonists, J. Med. Chem. 46 (2003) 4847–4859.

[15] J.J. Ruprecht, T. Mielke, R. Vogel, C. Villa, G.F.X. Schertler, Electron crystallography reveals the structure of metarhodopsin I, EMBO J. 23 (2004) 3609–3620.

[16] Z.-G. Gao, J. Blaustein, A.S. Gross, N. Melman, K.A. Jacobson, N^6-Substituted adenosine derivatives: selectivity, efficacy, and species differences at A_3 adenosine receptor, Biochem. Pharmacol. 65 (2003) 1675–1684.

[17] M. Ohno, Z.-G. Gao, P. Van Rompaey, S. Tchilibon, S.-K. Kim, B.A. Harris, A.S. Gross, H.T. Duong, S. Van Calenbergh, K.A. Jacobson, Modulation of adenosine receptor affinity and intrinsic efficacy in adenine nucleosides substituted at the 2-position, Bioorg. Med. Chem. 12 (2004) 2995–3007.

[18] S. Tchilibon, S.-K. Kim, Z.-G. Gao, B.A. Harris, J.B. Blaustein, A.S. Gross, H.T. Duong, N. Melman, K.A. Jacobson, Exploring distal regions of the A_3 adenosine receptor binding site: sterically constrained N^6-(2-phenylethyl)adenosine derivatives as potent ligands, Bioorg. Med. Chem. 12 (2004) 2021–2034.

[19] K.A. Jacobson, X.-D. Ji, A.-H. Li, N. Melman, M.A. Siddiqui, K.-J. Shin, V.E. Marquez, R.G. Ravi, Methanocarba analogues of purine nucleosides as potent and selective adenosine receptor agonists, J. Med. Chem. 43 (2000) 2196–2203.

[20] E.W. van Tilburg, J. von Frijtag Drabbe Künzel, M. de Groote, R.C. Vollinga, A. Lorenzen, A.P. IJzerman, N^6, 5′-Disubstituted adenosine derivatives as partial agonists for the human adenosine A_3 receptor, J. Med. Chem. 42 (1999) 1393–1400.

[21] Z.-G. Gao, B.V. Joshi, A.M. Klutz, S.-K. Kim, H.W. Lee, H.O. Kim, L.S. Jeong, K.A. Jacobson, Conversion of A_3 adenosine receptor agonists into selective antagonists by modification of the 5′-ribofuran-uronamide moiety, Bioorg. Med. Chem. Lett. 16 (2006) 596–601.

[22] Z.-G. Gao, L.S. Jeong, H.R. Moon, H.O. Kim, W.J. Choi, D.H. Shin, E. Elhalem, M.J. Comin, N. Melman, L. Mamedova, A.S. Gross, J.B. Rodriguez, K.A. Jacobson, Structural determinants of efficacy at A_3 adenosine receptors: modification of the ribose moiety, Biochem. Pharmacol. 67 (2004) 893–901.

[23] S. Tchilibon, B.V. Joshi, S.-K. Kim, H.T. Duong, Z.-G. Gao, K.A. Jacobson, (*N*)-Methanocarba, 2, N^6-disubstituted adenine nucleosides as highly potent and selective A_3 adenosine receptor agonists, J. Med. Chem. 48 (2005) 1745–1758.

[24] K.-Y. Jung, S.-K. Kim, Z.-G. Gao, A.S. Gross, N. Melman, K.A. Jacobson, Y.-C. Kim, Structure-activity relationships of thiazole and thiadiazole derivatives as potent and selective human adenosine A_3 receptor antagonists, Bioorg. Med. Chem. 12 (2004) 613–623.

[25] V. Colotta, D. Catarzi, F. Varano, F.R. Calabri, O. Lenzi, G. Filacchioni, C. Martini, L. Trincavelli, F. Deflorian, S. Moro, 1,2,4-Triazolo[4,3-a]quinoxalin-1-one moiety as an attractive scaffold to develop new potent a selective human A_3 adenosine receptor antagonists: synthesis, pharmacological, and ligand receptor modeling studies, J. Med. Chem. 47 (2004) 3580–3590.

[26] S.W. Lin, T.P. Sakmar, Specific tryptophan UV-absorbance changes are probes of the transition of rhodopsin to its active state, Biochemistry 35 (1996) 11149–11159.

[27] A.J. Bridges, R.F. Bruns, D.F. Ortwine, S.R. Priebe, D.L. Szotek, B.K. Trivedi, N^6-(R)-[2-(3,5-dimethoxyphenyl)-2-(2-methylphenyl)ethyl]adenosine and its uronamide derivatives. Novel adenosine agonists with both high affinity and high selectivity for the adenosine A_2 receptor, J. Med. Chem. 31 (1988) 1282–1285.

[28] V. Ozola, M. Thorand, M. Diekmann, R. Qurishi, B. Schumacher, K.A. Jacobson, C.E. Müller, 2-Phenylimidazo[2,1-i]purin-5-ones: structure-activity relationships and characterization of potent and selective inverse agonists at human A_3 adenosine receptors, Bioorg. Med. Chem. 11 (2003) 347–356.

[29] P.G. Baraldi, B. Cacciari, R. Romagnoli, G. Spalluto, S. Moro, K.-N. Klotz, E. Leung, K. Varani, S. Gessi, S. Merighi, P.A. Borea, Pyrazolo[4,3-e]1,2,4-triazolo[1,5-c]pyrimidine derivatives as highly potent and selective human A_3 adenosine receptor antagonists: influence of the chain at the N^8 pyrazole nitrogen, J. Med. Chem. 43 (2000) 4768–4780.

[30] Z.-G. Gao, S.-K. Kim, A.S. Gross, A. Chen, J.B. Blaustein, K.A. Jacobson, Identification of essential residues involved in the allosteric modulation of the human A_3 adenosine receptor, Mol. Pharmacol. 63 (2003) 1021–1031.

[31] Y. Liang, D. Fortiadis, S. Filipek, D.A. Saperstein, K. Palczewski, A. Engel, Organization of the G protein-coupled receptors rhodopsin and opsin in native membranes, J. Biol. Chem. 278 (2003) 21655–21662.

[32] W. Guo, L. Shi, M. Filizola, H. Weinstein, J. Javitch, Crosstalk in G protein-coupled receptors: changes at the transmembrane homodimer interface determine activation, Proc. Natl. Acad. Sci. U.S.A. 102 (2005) 17495–17500.

[33] S.D.C. Ward, F.F. Hamdan, L.M. Bloodworth, J. Wess, Conformational changes that occur during M_3 muscarinic acetylcholine receptor activation probed by the use of an *in situ* disulfide cross-linking strategy, J. Biol. Chem. 277 (2002) 2247–2257.

[34] S.-J. Han, S.-K. Kim, F. Hamdan, K.A. Jacobson, L.M. Bloodworth, B. Li, J. Wess, Identification of an agonist-induced conformational change occurring adjacent to the ligand binding pocket of the M_3 muscarinic acetylcholine receptor, J. Biol. Chem. 280 (2005) 34849–34858.

[35] T. Mirzadegan, G. Benko, S. Filipek, K. Palczewski, Sequence analyses of G-protein-coupled receptors: similarities to rhodopsin, Biochemistry 42 (2003) 2759–2767.

[36] J. Li, P.C. Edwards, M. Burghammer, C. Villa, G.F.X. Schertler, Structure of bovine rhodopsin in a trigonal crystal form, J. Mol. Biol. 343 (2004) 1409–1438.

[37] U. Gether, S. Lin, P. Ghanouni, J.A. Ballesteros, H. Weinstein, B.K. Kobilka, Agonists induce conformational changes in transmembrane domains III and VI of the β_2 adrenoceptor, EMBO J. 16 (1997) 6737–6747.

[38] F.F. Hamdan, S.D.C. Ward, N.A. Siddiqui, L.M. Bloodworth, J. Wess, Use of an in *situ* disulfide cross-linking strategy to map proximities between amino acid residues in transmembrane domains I and VII of the M_3 muscarinic acetylcholine receptor, Biochemistry 41 (2002) 7647–7658.

[39] S.-J. Han, F.F. Hamdan, S.-K. Kim, K.A. Jacobson, L. Brichta, L.M. Bloodworth, J.H. Li, J. Wess, Pronounced conformational changes following agonist activation of the M_3 muscarinic acetylcholine receptor, J. Biol. Chem. 280 (2005) 24870–24879.

[40] B. Kobilka, Agonist-induced conformational changes in the β_2 adrenergic receptor, J. Pept. Res. 60 (2002) 317–321.

[41] W.P. Clarke, R.S. Bond, The exclusive nature of intrinsic efficacy, Trends Pharmacol. Sci. 19 (1998) 270–276.

[42] S. Merighi, K. Varani, S. Gessi, K.N. Klotz, E. Leung, P.G. Baraldi, P.A. Borea, Binding thermodynamics at the human A_3 adenosine receptor, Biochem. Pharmacol. 63 (2002) 157–161.

[43] SYBYL®, version 7.0, Tripos Inc., 1699 South Hanley Rd., St. Louis, Missouri 63144, USA.

[44] T.A. Halgren, MMFF VII. Characterization of MMFF94, MMFF94s, and other widely available force fields for conformational energies and for intermolecular-interaction energies and geometries, J. Comput. Chem. 20 (1999) 730–748.

[45] J.J.P. Stewart, MOPAC: a semiempirical molecular orbital program, J. Comput. Aid. Mol. Des. 4 (1990) 1–105.

[46] Y. Martin, M. Burses, E. Dahaner, J. DeLazzer, I. Lico, P. Pavlik, A fast approach to pharmacophore mapping and its application to dopaminergic and benzodiazepine agonists, J. Comput. Aid. Mol. Des. 7 (1993) 83–102.

[47] M. Rarey, B. Kramer, T. Lengauer, G. Klebe, A fast flexible docking method using an incremental construction algorithm, J. Mol. Biol. 261 (1996) 470–489.

[48] G. Klebe, T. Mietzner, A fast and efficient method to generate biologically relevant conformations, J. Comput. Aid. Mol. Des. 8 (1994) 583–606.

[49] J.P. Ryckaert, G. Ciccotti, H.J.C. Berendsen, Numerical integration of the Cartesian equations of motion for a system with constraints: molecular dynamics of n-alkanes, J. Comput. Phys. 23 (1977) 327–333.

[50] A.-H. Li, S. Moro, N. Forsyth, N. Melman, X.-D. Ji, K.A. Jacobson, Synthesis, CoMFA analysis, and receptor docking of 3,5-diacyl-2,4-dialkylpyridine derivatives as selective A_3 adenosine receptor antagonists, J. Med. Chem. 42 (1999) 706–721.

[51] Y.-C. Kim, M. de Zwart, L. Chang, S. Moro, J.K. van Frijtag Prabbe Künzel, N. Melman, A.P. IJzerman, K.A. Jacobson, Derivatives of the triazoloquinazoline adenosine antagonist (CGS15943) having high potency at the human A_{2B} and A_3 receptor subtypes, J. Med. Chem. 41 (1998) 2835–2845.

[52] M.H. Lim, H.O. Kim, H.R. Moon, S.J. Lee, M.W. Chun, Z.-G. Gao, N. Melman, K.A. Jacobson, J.H. Kim, L.S. Jeong, Design, synthesis and binding affinity of 3′-fluoro analogues of Cl-IB-MECA as adenosine A_3 receptor ligands, Bioorg. Med. Chem. Lett. 13 (2003) 817–820.

[53] B.B. Fredholm, E. Irenius, B. Kull, G. Schulte, Comparison of the potency of adenosine as an agonist at human adenosine receptors expressed in Chinese hamster ovary cell, Biochem. Pharmacol. 61 (2001) 443–448.